J|A|C|S
ARTICLES
Published on Web 11/21/2006

22π Smaragdyrin Molecular Conjugates with Aromatic Phenylacetylenes and Ferrocenes: Syntheses, Electrochemical, and Photonic Properties

Rajneesh Misra,[†] Rajeev Kumar,[†] Tavarekere K. Chandrashekar,*[,†,‡] C. H. Suresh,[‡] Amit Nag,[†] and Debabrata Goswami[†]

Contribution from the Department of Chemistry, Indian Institute of Technology, Kanpur 208016, India, and Regional Research Laboratory, Trivandrum, Kerala 695019, India

Received April 24, 2006; E-mail: tkc@iitk.ac.in

Abstract: Syntheses, spectroscopic, electrochemical, and third-order nonlinear optical susceptibilities of a series of 22π smaragdyrins and their corresponding Rh(I) derivatives bearing phenylacetylene substituents and ferrocene-containing substituents are reported. The synthetic strategy involved a [3 + 2] acid-catalyzed oxidative coupling reaction of the appropriate dipyrromethane and oxatripyrrane. The desired meso substituents, such as phenylacetylenylphenyl and the ferrocenes, were incorporated to the dipyrromethane unit prior to the oxidative coupling reaction. The optical absorption, emission characteristics, and the quantum yield of the smaragdyrin conjugates depends on the nature of the substituent, nature of linker group, and the spacer length. Theoretical studies at the DFT level suggest high delocalization of electrons confined to only four of the five available heterocyclic rings for the free bases. However, upon Rh(I) metalation, the π-electron delocalization is extended to all the heterocyclic rings. The two-photon absorption cross section (TPA) values $\sigma^{(2)}$ measured through the open aperture *Z*-scan method, increases linearly with enhanced π-electron delocalization for the smaragdyrins containing phenylacetylene substituents. The meta branching of substituents decreases $\sigma^{(2)}$ values. Introduction of Rh(I) to the smaragdyrin cavity enhances the $\sigma^{(2)}$ values by about 3−10 orders of magnitude, attributed to the increased aromatic character upon Rh(I) insertion. The calculated molecular electrostatic potential (MESP) and harmonic oscillator model of aromaticity (HOMA) for the free bases and the Rh(I) derivatives justifies such a conclusion. A linear correlation observed for the second oxidation potential of Rh(I) derivatives and corresponding free bases also support the increased aromaticity upon Rh(I) insertion. The electrochemical data for ferrocene-containing smaragdyrins reveal easier ring oxidation by about 50−130 mV and harder ferrocene oxidation by 40−180 mV suggesting electron-donating nature of the ferrocene upon linking with the smaragdyrin π system. The TPA cross section value of 88782 GM observed for **5g** represents one of the highest values known for a metalloexpanded porphyrin derivative.

I. Introduction

Organic molecules capable of exhibiting large nonlinear optical susceptibilities have attracted the attention of chemists because of their diverse technological applications.[1] The presence of large π-electron delocalization and a flat structure are the key elements in the design of organic molecules for nonlinear optical applications.[2] Recent research on such molecules is aimed at an understanding of structure−function correlation. Various organic molecules, which contain π-conjugated electrons with appropriate donor−acceptor groups, organic dyes based on hetroaromatics,[3] and dendritic systems containing triphenylamine[4] and anthracene derivatives[5] have been tried for nonlinear optical applications. Another important class of organic molecules, which have attracted the attention of chemists for application in nonlinear optics is the porphyrin and expanded porphyrin systems. These systems are popular because of their π-electron delocalization, flat structure, high thermal stability, and flexible molecular design. For example fused diporphyrins,[6] meso−meso and alkyne-linked porphyrins,[7] butadiyne-linked self-assembled porphyrins,[8] and aggregated porphyrins[9] have been investigated for their third-order nonlinear optical response

[†] Indian Institute of Technology.

[‡] Present address: Regional Research Laboratory, Trivandrum, Kerala 695 019.

(1) (a) Marder, S. R.; Kippelen, B.; Jen, A. K.-Y.; Peyghambarian, N. *Nature* **1997**, *388*, 845. (b) Zhou, W.; Kuebler, S. M.; Braun, K. L.; Yu, T.; Cammack, J. K.; Ober, C. K.; Perry, J. W.; Marder, S. R. *Science* **2002**, *296*, 1106.

(2) Torre, G. de la; Vazquez, P.; Lopez, F. A.; Torres, T. *Chem. Rev.* **2004**, *104*, 3723.

(3) Abbotto, A.; Beverina, L.; Bozio, R.; Facchetti, A.; Ferrante, C.; Pagani, G. A.; Pedron, D.; Signorini, R. *Org. Lett.* **2002**, *4*, 1495.

(4) Wei, P.; Bi, X.; Wu, Z. *Org. Lett.* **2005**, *7*, 3199.

(5) Lee, S. K.; Yang, W. S.; Choi, J. J.; Kim, C. H.; Jeon, S. J.; Cho, B. R. *Org. Lett.* **2005**, *7*, 323.

(6) Kim, D. Y.; Ahn, T. K.; Kwon, J. H.; Kim, D.; Ikeue, T.; Aratani, A.; Osuka, A.; Shigeiwa, M.; Maeda, S. *J. Phys. Chem. A* **2005**, *109*, 2996.

(7) (a) Inokuma, Y.; Ono, N.; Uno, H.; Kim, D. Y.; Noh, S. B.; Kim, D.; Osuka, A. *Chem. Commun.* **2005**, 3782. (b) Drobizhev, M.; Stepanenko, Y.; Dzenis, Y.; Karotki, A.; Rebane, A.; Taylor, P. N.; Anderson, H. L. *J. Am. Chem. Soc.* **2004**, *126*, 15352. (c) Drobizhev, M.; Stepanenko, Y.; Dzenis, Y.; Karotki, A.; Rebane, A.; Taylor, P. N.; Anderson, H. L. *J. Phys. Chem. B* **2005**, *109*, 7223.

10.1021/ja0628295 CCC: $33.50

using TPA cross section measurements. In these systems the $\sigma^{(2)}$ values are in the range of 100−15000 GM. Very recently Kim and Osuka and co-workers have reported $\sigma^{(2)}$ values for fused tetramericporphyrinic sheet and porphyrin dimers and trimers where the large $\sigma^{(2)}$ value of the order of 93600 GM has been observed.[10] For a better understanding of the correlation between TPA cross section values and the molecular structure of porphyrins and expanded porphyrins, more studies on diverse porphyrin architecture are essential. Very recently, we have reported large $\sigma^{(2)}$ values of expanded porphyrins[11] containing 26π and 34π electrons. In continuation of our studies on the structure−function correlation, in this paper we wish to report the syntheses, characterization, spectrochemical, and electrochemical properties as well as TPA cross section values of a series of 22π smaragdyrin with diverse meso substituents.

We have chosen two different types of meso substituents in this study. In the first category a series of phenylacetylene and diphenylacetylene spacers are linked at the meso position of the 22π smaragdyrin to understand the effect of enhanced π conjugation on $\sigma^{(2)}$ values.[12] In the second category an electroactive group like ferrocene is either linked directly to the meso position of the smaragdyrin skeleton or the linking has been done through phenylacetylene spacers. It has been shown that the linking of meso substituents enhances the π-electron conjugation between the smaragdyrin π system and the meso substituents resulting in enhanced TPA cross section values. Furthermore, metalation of the smaragdyrin skeleton with Rh(I) also enhances the $\sigma^{(2)}$ values due to increased aromatic character. Geometry optimization and calculation of molecular electrostatic potential (MESP) support the increased aromatic character upon the introduction of Rh(I).

II. Results

A. Syntheses. For the synthesis of smaragdyrins with spacers, two new aldehydes which are unknown in the literature were synthesized using the Sonogashira coupling reaction (Scheme 1). Typically, ethynylferrocene **6** and ethynylphenylferrocene **7** were reacted with 3-iodobenzaldehyde under the sonogashira condition to get aldehyde **1i** and **1k**, respectively, in 89% yield.

Further, the required smaragdyrin **4** was synthesized by a well-known acid-catalyzed [3 + 2] oxidative coupling methodology[13] using dipyrromethane **2** with the appropriate R group and oxatripyrrane **3** followed by chloranil oxidation (Scheme 2). The desired product was separated by silica gel column chromatography using dichloromethane as solvent. The smaragdyrins **4a**−**4k** were found to be stable both in solid and solution phase in their free-base form. The Rh(I) complexes **5a**−**5k** were synthesized by the reaction of the corresponding free bases **4a**−**4k** with di-μ-chlorobis[dicarbonylrhodium(I)] in the presence of sodium acetate. The purification was performed with silica gel column chromatography, where the intense green color fraction was isolated as a pure product. The metal complexes were quite stable at room temperature.

Scheme 1. Syntheses of New Aldehydes

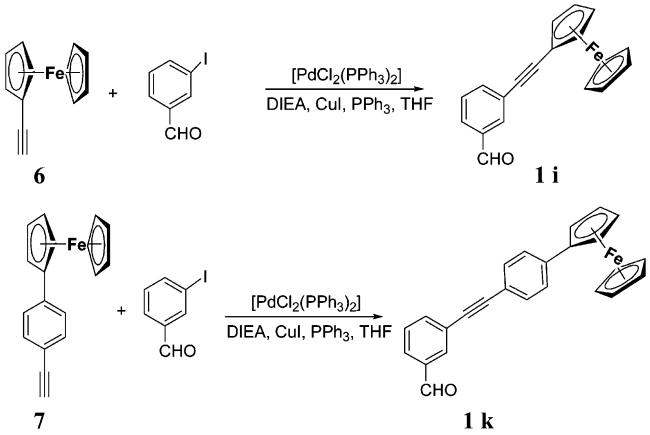

B. Structural Analysis by ^{1}H NMR. The structure elucidation of the various smaragdyrin molecular conjugates in solution has been done through a detailed analysis of ^{1}H and 2D NMR spectra. In general, ^{1}H NMR spectra of conjugates were well resolved both in the free base as well as in the metallated form. A typical spectra of **4a** is shown in Figure 1, and the assignments are marked. Briefly, the bipyrrole protons (b, b′; c, c′; d, d′; e, e′) resonate as four well-resolved doublets in the region of 8−10 ppm with coupling constants of 4−4.4 Hz. The outer pyrrolic protons (b, b′; e, e′) are more shielded compared to the inner pyrrolic protons (c, c′; d, d′) because of the upfield ring current contribution of the meso aryl ring. The β-CH protons of the furan ring (a, a′) appear as a sharp singlet at 8.54 ppm, while the meso hydrogen (f) resonates as sharp singlet at 9.83 ppm. The equivalence of these pyrrolic protons (b, b′; c, c′; d, d′; e, e′) in the ^{1}H NMR spectrum suggests that the molecule adopts a symmetric conformation in solution with respect to the mirror plane passing through the methine bridge connecting the meso free hydrogen and the furan oxygen atom. This is possible only if there is a rapid tautomerism between the inner −NH protons indicating the three −NH protons exchange sites between four bipyrrole nitrogen centers. Upon lowering the temperature to 240 K, no −NH signals were observed, indicating tautomerism even at 240 K.

Treatment of the free-base smaragdyrins with di-μ-chlorobis-[dicarbonylrhodium(I)] gives the corresponding Rh(I) salt of the smaragdyrins, where Rh is bound in an η^2 fashion to the pyrrole nitrogens of dipyrromethane unit, with the other two coordination sites on Rh taken by ancillary carbonyl groups.[16] A representative ^{1}H/^{1}H COSY spectrum observed for **5c** is depicted, and assignments are marked (Figure 2). The metalation with rhodium arrests the NH tautomerism and the −NH protons, which are not coordinating to rhodium metal, now appear as a singlet at −1.60 ppm, supporting the presence of NH tautomerism in the free base.

After metalation the pyrrolic protons (b, b′; c, c′) appear as quartets (J = 2.2 Hz), which in the free base was a doublet,

(8) Ogawa, K.; Ohashi, A.; Kobuke, Y.; Kamada, K.; Ohta, K. *J. Am. Chem. Soc.* **2003**, *125*, 13356.
(9) Collini, E.; Ferrante, C.; Bozio, R. *J. Phys. Chem. B* **2005**, *109*, 2.
(10) (a) Ahn, T. K.; Kim, K. S.; Kim, D. Y.; Noh, S. B.; Aratani, N.; Ikeda, C.; Osuka, A.; Kim, D. *J. Am. Chem. Soc.* **2006**, *128*, 1700. (b) Nakamura, Y.; Aratani, N.; Shinokuba, H.; Takagi, A.; Kawai, T.; Matsumoto, T.; Yoon, Z. S.; Kim, D. Y.; Ahn, T. K.; Kim, D.; Muranaka, A.; Kobayashi, N.; Osuka, A. *J. Am. Chem. Soc.* **2006**, *128*, 4119.
(11) Rath, H.; Sankar, J.; Prabhuraja, V.; Chandrashekar, T. K.; Nag, A.; Goswami, D. *J. Am. Chem. Soc.* **2005**, *127*, 11608.
(12) Misra, R.; Kumar, R.; Chandrashekar, T. K.; Nag, A.; Goswami, D. *Org. Lett.* **2006**, *8*, 629.
(13) Narayanan, S. J.; Sridevi, B.; Chandrashekar, T. K.; Englich, U.; Senge, K. R. *Org. Lett.* **1999**, *1*, 587.
(14) Chandrashekar, T. K.; Venkatraman, S. *Acc. Chem. Res.* **2003**, *36*, 676−691.
(15) Melinger, J. S.; Pan, Y.; Kleiman, V. D.; Peng, Z.; Davis, B. L.; McMorrow, D.; Lu, M. *J. Am. Chem. Soc.* **2002**, *124*, 12002.
(16) This conclusion is based on our earlier single-crystal X-ray structural studies on the Rh^{I} complex of oxa smaragdyrins; for details see ref 17.

Scheme 2. Syntheses of Smaragdyrins and Their Rh(I) Derivatives

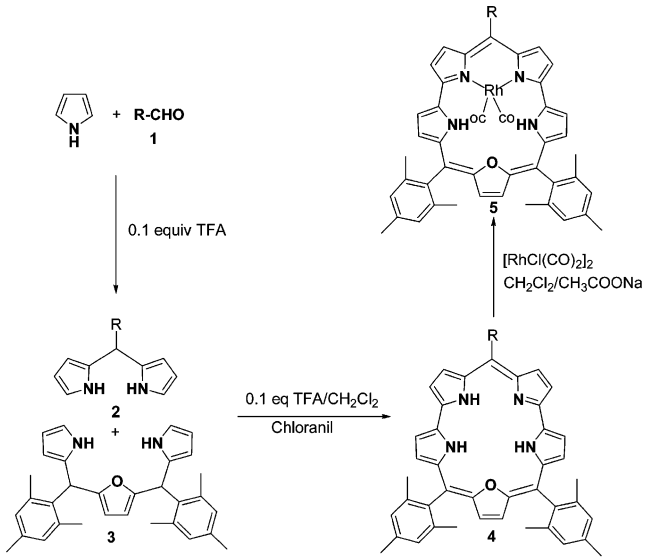

entry	R-CHO (**1**)	dipyrromethane (**2**)	smaragdyrin (**4**)	Rh salt of smaragdyrin(**5**)
1	H	**1a**	**2a**	**4a**	**5a**
2		**1b**	**2b**	**4b**	**5b**
3	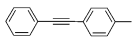	**1c**	**2c**	**4c**	**5c**
4	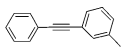	**1d**	**2 d**	**4 d**	**5 d**
5	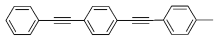	**1e**	**2e**	**4e**	**5e**
6	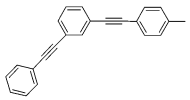	**1f**	**2f**	**4f**	**5f**
7		**1g**	**2g**	**4g**	**5g**
8	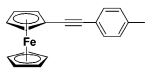	**1h**	**2h**	**4h**	**5h**
9	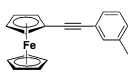	**1i**	**2i**	**4i**	**5i**
10	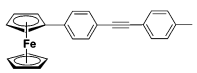	**1j**	**2j**	**4j**	**5j**
11	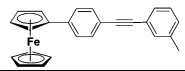	**1k**	**2k**	**4k**	**5k**

while the pyrrolic protons (d, d′; e, e′) remain as doublets (J = 4.2 Hz). This observation further confirms our earlier finding that Rh(I) prefers to bond to the bipyrrolic rings with one amino and one imino nitrogen.[18] The phenylacetylenylphenyl group at one of the meso positions has a total of four sets of protons; the protons present next to the carbon atom connected to the meso position (f, f′) resonate at δ = 8.28 ppm, the other two protons (g, g′) resonate at δ =7.98 ppm, while the other two

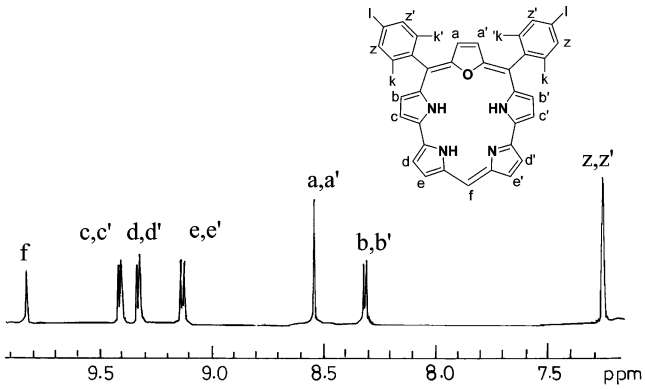

Figure 1. ^{1}H NMR spectrum of **4a** at 25 °C in $CDCl_3$. The assignments are also shown.

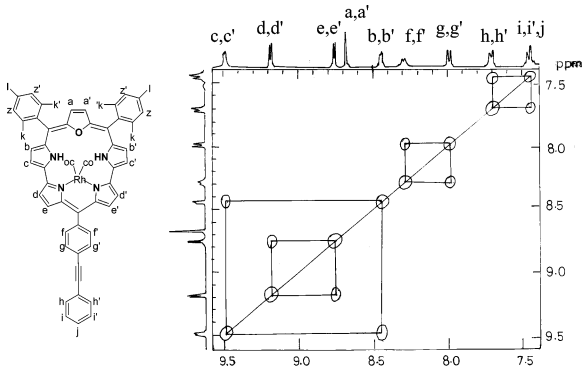

Figure 2. ^{1}H/^{1}H COSY spectrum of **5c** at 25 °C in $CDCl_3$. The observed correlations and assignment are marked.

sets of protons (h, h′) and (i, i′, j) appear at δ = 7.71 and 7.42, respectively.

C. Single-Photon Absorption and Emission Properties. The electronic absorption spectra of molecular conjugates and their Rh(I) metal derivatives show a typical intense Soret like band in the region of 440−464 nm and four Q bands in the region of 550−750 nm, suggesting the porphyrinic nature of macrocycles. The monoprotonation leads to a red shift (5−8 nm) in both the Soret and Q bands relative to the free-base form consistent with the meso aryl nature of smaragdyrins.[14] Typical electronic absorption spectra observed for **4a**, **4i**, and **5i** are shown in Figure 3, and the data are listed in Table 1.

An analysis of the data reveal the following. (1) Introduction of substituents at the meso free position results in a bathochromic shift of both the Soret and Q bands relative to those of **4a**. (2) Increasing the conjugation by substituting various phenylacetylene spacers results in a red shift of the absorption bands. The magnitude of the shifts is generally larger for the para isomer relative to that of the corresponding meta isomer, as it is known that meta substitution disrupts the extended π conjugation.[15] This result demonstrates that meta branching prevents an efficient delocalization of the electronic wave function over the conjugated backbone. (3) Metalation of the conjugates with Rh(I) salt shifts the absorption maxima to the red by about 10−25 nm and the emission maxima by about 10−15 nm. (4) Metalation results in the quenching of fluorescence intensity resulting in the decreased quantum yield. For example, the quantum yield of **4e** is 0.120 while that of the corresponding Rh derivative **5e** is 0.002. (5) In the ferrocene-containing smaragdyrins, the direct linking of ferrocene at the meso position quenches the fluorescence completely, while when

(17) Sridevi, B.; Narayanan, S. J.; Rao, R.; Chandrashekar, T. K.; Englich, U.; Senge, K. R. *Inorg. Chem.* **2000**, *39*, 3669.
(18) Narayanan, S. J.; Sridevi, B.; Chandrashekar, T. K.; Englich, U.; Senge, K. R. *Inorg. Chem.* **2001**, *40*, 1637.

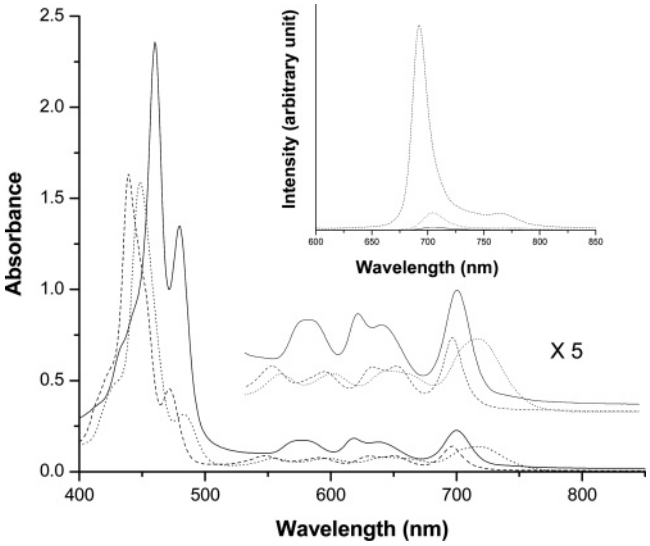

Figure 3. Electronic absorption spectrum of **4a** (- - -), **4i** (· · ·), and **5i** (—) in CH_2Cl_2. (The inset shows emission spectra of **4a** (- - -), **4i** (· · ·), and **5i** (—) in benzene.)

Table 1. Photophysical Data of Smaragdyrins in Benzene at 25 °C

compound	λ_{abs} (nm)	λ_{em} (nm)	stokes shift (cm^{-1})	quantum yield ϕ_f
4a	440, 471 (sh), 547, 590, 630, 696	692	8276	0.043
5a	454, 474 (sh), 567, 611, 631, 691	692	7575	0.002
4b	445, 554, 594, 638, 701	701	8206	0.049
5b	459, 479 (sh), 570, 616, 698	706	7622	0.002
4c	455, 486 (sh), 605, 659, 729	710	7893	0.104
5c	462, 480 (sh), 578, 620, 640	713	7619	0.040
4d	451, 483 (sh), 607, 661, 721	705	7988	0.073
5d	460, 479 (sh), 574, 619, 639, 701	705	7554	0.003
4e	457, 486 (sh), 614, 661, 729	713	7856	0.120
5e	463, 479 (sh), 617, 646, 703	711	7533	0.002
4f	452, 556, 597, 640, 705	711	8059	0.065
5f	462, 481 (sh), 581, 620, 705	710	7560	0.003
4g	451, 565, 606, 647, 712			
5g	464, 494, 588, 629, 656, 716			
4h	451, 556, 597, 641, 707	710	8088	0.003
5h	462, 480, 619, 701	710	7560	0.001
4i	448, 483, 554, 597, 644, 716	704	8116	0.013
5i	460, 480, 578, 618, 637, 700	703	7514	0.002
4j	455, 485, 556, 601, 657, 729	711	7913	0.020
5j	462, 480, 572, 619, 703	713	7619	0.003
4k	450, 483, 554, 597, 646, 720	704	8017	0.031
5k	463, 481, 574, 653, 722	704	7393	

ferrocene is linked via a spacer group the smaragdyrins regain the fluorescence and the fluorescence intensity depends upon the spacer length. For example, **4g** is nonfluorescent, for **4h** the quantum yield is 0.003, while for **4j** it is 0.020. (6) The quantum yield is also dependent on the number of phenylacetylene groups at the meso position, and quantum yield increases linearly with the spacer length due to increased π conjugation. For example, for **4a**, **4b**, **4c**, and **4e** the quantum yields are 0.043, 0.049, 0.104, and 0.120. The meta branching at the phenylacetylene unit decreases the quantum yield due to disruption of the extended π-electron conjugation.

D. Electrochemical Studies. The redox behavior of various conjugates was monitored by cyclic voltammetric studies using 0.1 M $TBAPF_6$ (tetra *n*-butylammonium hexafluorophosphate) as the supporting electrolyte in CH_2Cl_2 in the potential range of 0−1.2 V versus the standard calomel electrode. Electrochemical data of the conjugates, their Rh(I) derivatives, and ferrocene are listed in Table 2. Some representative cyclic voltammograms overlaid with differential pulsed voltammograms are shown in Figure 4.

Table 2. Electrochemical Data for Smaragdyrins along with Free Ferrocene Using 0.1 M $TBAF_6$ (Tetra *n*-Butylammonium Hexafluorophosphate) as the Supporting Electrolyte in CH_2Cl_2, Potential Scanned from 0−1.2 V versus SCE Recorded at 100 mV/s Scan Speed

	expanded ring		ferrocenyl ring
compound	$E_{1/2}^{Ox}(1)$ [V]	$E_{1/2}^{Ox}(2)$ [V]	$E_{1/2}^{Ox}$ [V]
4a	0.344	0.696	
5a	0.392	0.844	
4b	0.372	0.716	
5b	0.412	0.848	
4c	0.328	0.688	
5c	0.392	0.820	
4d	0.360	0.704	
5d	0.412	0.844	
4e	0.308	0.636	
5e	0.348	0.784	
4f	0.340	0.684	
5f	0.404	0.828	
4g	0.240	0.832	0.492
5g	0.256	0.940	0.544
4h	0.308	0.668	0.496
5h	0.416	0.808	0.472
4i	0.312	0.668	0.500
5i	0.384	0.812	0.490
4j	0.312	0.652	0.409
5j	0.384	0.776	
4k	0.312	0.652	0.406
ferrocene			0.365

In general, smaragdyrins without meso ferrocene substituents give two redox couples on scanning toward positive potential due to the ring oxidations. However, smaragdyrins bearing ferrocenyl groups should give three redox couples, of which two correspond to smaragdyrin ring oxidations and the third one is attributable to the ferrocene oxidation.

From the Table 2 the following observations are apparent. (1) Increasing the conjugation by introducing a phenylacetylene unit from one to two at the meso position of smaragdyrin decreases the oxidation potential linearly suggesting easier oxidation. (2) The effect of meta versus para substituents on the phenyl ring also has an affect on oxidation potentials, where the meta isomers are slightly harder to oxidize relative to the para isomer. (3) Introduction of Rh(I) metal to the smaragdyrin cavity makes the oxidations harder relative to the free base probably due to lowering of symmetry.

Ferrocene-containing smaragdyrins (Figure 4) **4h** and **4i** show three oxidation couples as expected. Analysis of the data (Table 2) suggests the following: (a) Introduction of the ferrocene moiety at the meso carbon of the smaragdyrin ring shifts the first oxidation potential to less positive values implying easier oxidation upon ferrocene substitution. This is possible only when the ferrocene group is acting as an electron donor, pumping electron density toward the smaragdyrin π system. However, the magnitude of the decrease depends upon the spacer length, and maximum effects are seen when ferrocene is directly linked to the π system without any spacer. (b) The second ring oxidation is sensitive only when the ferrocene is linked directly, while these potentials are insensitive when the spacer is introduced between the smaragdyrin and ferrocene moiety. (c) On the other hand the ferrocene oxidation potential as expected shows harder oxidation relative to that of free ferrocene

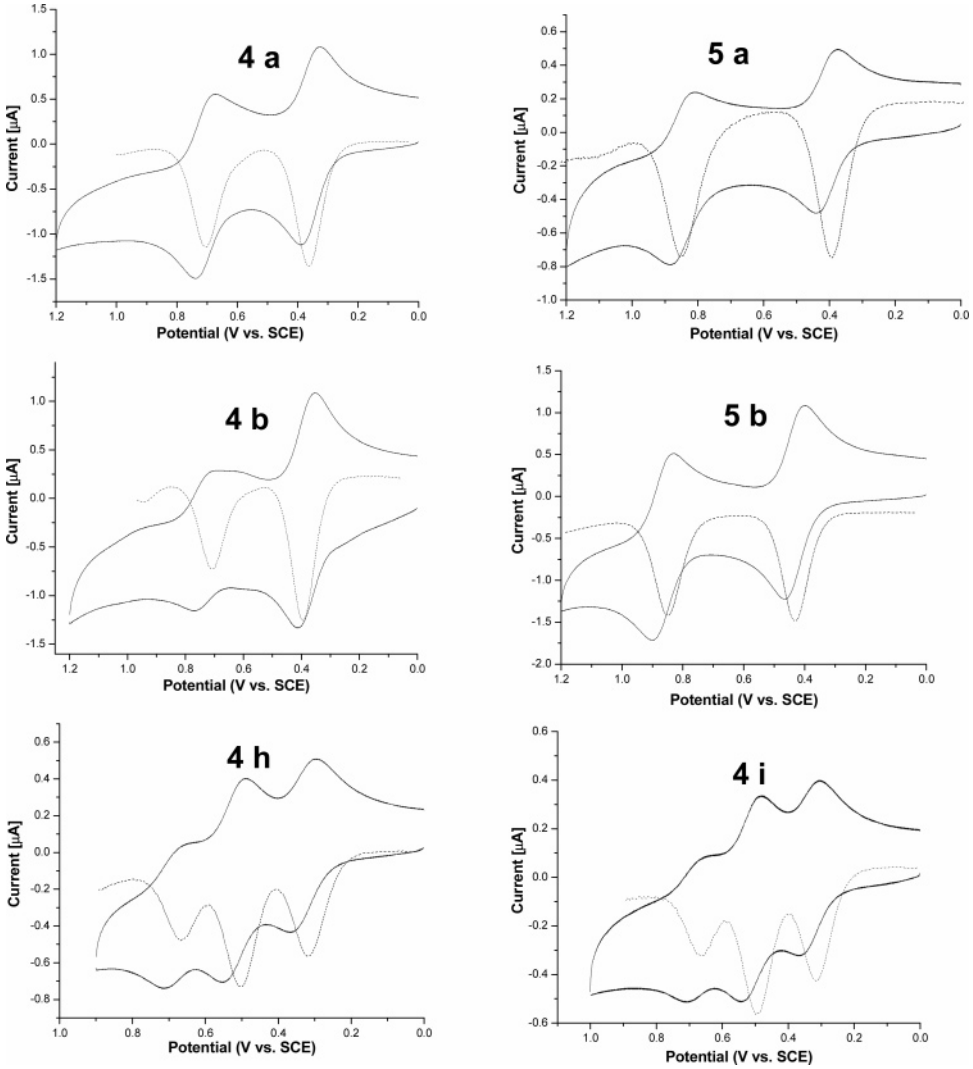

Figure 4. Cyclic voltammograms (—) and differential pulse voltammograms (- - -) of **4a**, **5a**, **4b**, **5b**, **4h**, and **4i** in CH_2Cl_2 containing 0.1 M $TBAPF_6$, recorded at a 100 mV/s scan speed.

confirming the electron-donating nature of ferrocene. Here also the maximum effect (130 mV shift) is seen when ferrocene is directly linked to the π system. (d) Metalation with Rh(I) results in a shifting of potential of both the ring and ferrocene oxidation toward more positive values, consistent with our earlier observation.[19] Thus, the electrochemical study reveals that the electronic communication between the ferrocene moiety and smaragdyrin ring depends on both the nature of the spacer as well as the length of spacer.

E. Two-Photon Absorption Properties. The third-order nonlinear optical properties of the conjugates and their Rh(I) derivatives were followed through measurement of TPA cross section values using the open aperture *Z*-scan method. The TPA spectra were measured either at 780 or 830 nm at which the one-photon absorption spectral intensity is nearly zero. The TPA values measured at 100 and 150 fs pulse width are listed in Table 3; Figure 5 shows a typical open aperture *Z*-scan trace obtained for **5b**, **5g**, **5h**, and **5j**.

An analysis of the TPA cross section data reveals: (1) the $\sigma^{(2)}$ value increases with conjugation length, the nature of the substitution (para vs meta), and the number of phenylacetylene units attached to the meso phenyl of the smaragdyrin skeleton. In general, the para isomer shows a larger $\sigma^{(2)}$ value as compared to that of the meta isomer. (2) For the ferrocene-containing smaragdyrins, $\sigma^{(2)}$ values are larger relative to those of the phenylacetylene system, and the highest values are seen for **4j** and **4k**, where the ferrocene is linked through phenylacetylene spacers. (3) There is a large enhancement of the $\sigma^{(2)}$ values upon Rh metalation, and the highest value of 88782 GM is observed for **5g** in which the ferrocene is linked directly to the smaragdyrin π system.

F. Optimized Geometries and Aromatic Character of Smaragdyrin Systems. For an understanding of the structure−function correlation, a detailed structure of smaragdyrin conjugates described in the study is essential. Failure to obtain good quality crystals forced us to resort to geometry optimization at the BLYP level of density functional theory to get the structural information.[20,21] Systems **4a**−**4e**, **4g**, **4h**, **4i**, and **5b** were selected for the theoretical study. The optimized geometry of **4b** and **4h** are presented in Figure 6. For the remaining free bases, the important structural features observed for the sma-

(19) Kumar, R.; Misra, R.; PrabhuRaja, V.; Chandrashekar, T. K. *Chem. Eur. J.* **2005**, *11*, 5695.

(20) Becke, A. D. *Phys. Rev. A* **1988**, *38*, 3098.
(21) Lee, C.; Yang, W.; Parr, R. G. *Phys. Rev. B* **1988**, *37*, 785.

Table 3. TPA Cross Section Values of Smaragdyrin Conjugates and Their Rh(I) Derivatives Measured by Femtosecond Laser Pulses[a]

compound	$\sigma^{(2)}$ (GM)	wavelength (nm)	pulse width (fs)
4a	986	830	150
5a	27643	830	150
4b	1086	830	150
5b	45260	830	150
4c	1215	780	100
5c	4496	780	100
4d	926	780	100
5d	1537	780	100
4e	7839	780	100
5e	15525	780	100
4f	6226	780	100
5f	10523	780	100
4g	5677	830	150
5g	88782	830	150
4h	3424	830	150
5h	66408	830	150
4i	1803	830	150
5i	22923	830	150
4j	16310	830	150
5j	45840	830	150
4k	13700	830	150
5k	39361	830	150

[a] The experimental uncertainty on $\sigma^{(2)}$ is of the order of 10%.

ragdyrin region are presented in Table 4. For rings **B**−**E**, the average value of the CC bond (CC_{ave}) and CN bond (CN_{ave}) is analyzed in all the cases. This analysis showed that irrespective of the substituent R, all the cases showed bond lengths around 1.400 Å for rings **B**−**E**. The bond length equalization phenomenon is considered as the geometric criterion of aromaticity,[22−24] and therefore, we can expect a high degree of π-electron delocalization in rings **B**−**E**, and most localized bonds are always present in ring **A** for all the free-base systems. Therefore, for all the "**4**" (free base) systems the best two-dimensional representation can be chosen as the schematic structure given in Figure 7. The presence of an intramolecular N···H hydrogen bond is a characteristic feature of all the "**4**" systems, which is located between the N−H hydrogen of ring **B** and the N of ring **A**. The N···H hydrogen bond is longest in the unsubstituted system **4a** (1.887 Å) and shortest in the ferrocene-linked **4g** system (1.808 Å). In all the other cases, this bond length is in the range of 1.834−1.838 Å, which means that the presence of the substituents strengthens the intramolecular hydrogen bond interaction. Further, all the "**4**" systems showed two intramolecular O···H distances in the range of 2.569−2.495 Å (Figure 6), which can be attributed to a stabilizing weak electrostatic interaction between the oxygen lone pair of the furan moiety and the N−H bonds of ring **C** and **E**.

Another structural feature noted in Table 4 is the twist angle (θ) between the plane of the macrocycle and the plane of the substituent ring moiety. The θ value is the smallest in the ferrocene-linked system (38.3°), and the rest showed this value in the range of 52.9−56.3°. All the systems with the para substituent connection showed a smaller twist than the system with the meta substituent connection, suggesting a slightly higher π conjugation in the former. The θ twist mainly arises due to the nonbonded H···H interactions given in the schematic structure (Figure 7), which is expected to be smaller when the connected R group is a five-membered cyclopentadienyl ring of a ferrocene moiety than a phenyl ring in the other systems, which explains the smaller θ twist in the ferrocene-connected system.

The optimized geometry of the 16-electron rhodium (I) complex **5b** depicted in Figure 8 shows a planar tetra-coordinate structure for the metal center. In this system, the rings **C**, **D**, and **E** are nearly in the same plane because the twist angles between rings **C** and **D** as well as rings **D** and **E** are only 2°. The twist angle between rings **A** and **E** is 12.4° and that between rings **B** and **C** is 9.8°, suggesting a small amount of puckering at the metal-coordinated rings **A** and **B**. Further, the bond length features of rings **B**−**E** are nearly identical to those of the "**4**" systems. On the other hand, the localized π-bonding features observed for the "**4**" systems at **A** ring (Figure 7) were absent in the **5b** because the shortest bond of length 1.381 Å in its **A** ring suggested a substantial amount of bond length equalization leading to aromatization of the ring.

A quantitative value of the aromaticity of the **A** ring is obtained by calculating the harmonic oscillator model of aromaticity (HOMA) index (see the Supporting Information for details).[22,23] In comparison to a HOMA value of 1 expected for a fully aromatic system, HOMA values of 0.467, 0.482, and 0.477 are obtained for the ring **A** of the meso free **4a**, benzene-linked **4b**, and ferrocene-linked **4g** metal-free systems, while in the case rhodium-coordinated **5b**, this value is 0.707. It may be noted that the HOMA value of pyrrole is 0.891 at the BLYP/6-31G* level, and therefore, we can assume that the coordination of rhodium to the smaragdyrin system leads to the enhancement of the π-electron delocalization in the system which extends through the rings **A**−**E**.

G. Molecular Electrostatic Potential Analysis. We have also calculated the molecular electrostatic potential (MESP) for the systems **4a**−**4e**, **4g**, **4h**, **4i**, and **5b** at their optimized level of theory. The MESP analysis is done by focusing mainly on the evaluation of its most negative-valued point (V_{min}) at various positions of the molecule. Such analysis is often used for understanding π-conjugation features, aromaticity, and the reactive behavior of molecules.[25−31] The MESP distributions of **4g** and **5b** are depicted using an isosurface of value −7.0 kcal/mol in Figure 9 (see the Supporting Information for the MESP features of other systems). In all the cases, the MESP isosurface spreads across the macrocycle and the substituent groups composed of the benzene ring, acetylenic bond, and the cyclopentadienyl ring of the ferrocene unit, and this revealed the extended π-electron conjugation in these systems. In all the systems, the **A** ring was the most electron-rich as it showed the most negative V_{min}, while the furan ring always showed the lowest negative V_{min}. Among all the systems, the most negative V_{min} is observed over the **A** ring of the ferrocene-linked **4g** system, and this result is indicative of the good electron-donating

(22) Krygowski, T. M.; Cyrañski, M. K. *Tetrahedron* **1996**, *52*, 1713.
(23) Krygowski, T. M.; Cyrañski, M. K.; Czarnocki, Z.; Hafelinger, G.; Katritzky, A. R. *Tetrahedron* **2000**, *56*, 1783.
(24) Suresh, C. H.; Koga, N. *Chem. Phys. Lett.* **2006**, *419*, 550.
(25) Politzer, P.; Truhlar, D. G. *Chemical Applications of Atomic and Molecular Electrostatic Potentials*; Plenum: New York, 1981.
(26) Gadre, S. R.; Shirsat, R. N. *Electrostatics of Atoms and Molecules*; Universities Press: Hyderabad, India, 2000.
(27) Murray, J. S.; Ranganathan, S.; Politzer, P. *J. Org. Chem.* **1991**, *56*, 3734.
(28) Luque, F. J.; Orozco, M.; Bhadane, P. K.; Gadre, S. R. *J. Phys. Chem.* **1993**, *97*, 9380.
(29) Bagdassarian, C. K.; Schramm, V. L.; Schwartz, S. D. *J. Am. Chem. Soc.* **1996**, *118*, 8825.
(30) Suresh, C. H.; Gadre, S. R. *J. Am. Chem. Soc.* **1998**, *120*, 7049.
(31) Suresh, C. H.; Gadre, S. R. *J. Org. Chem.* **1999**, *64*, 2505.

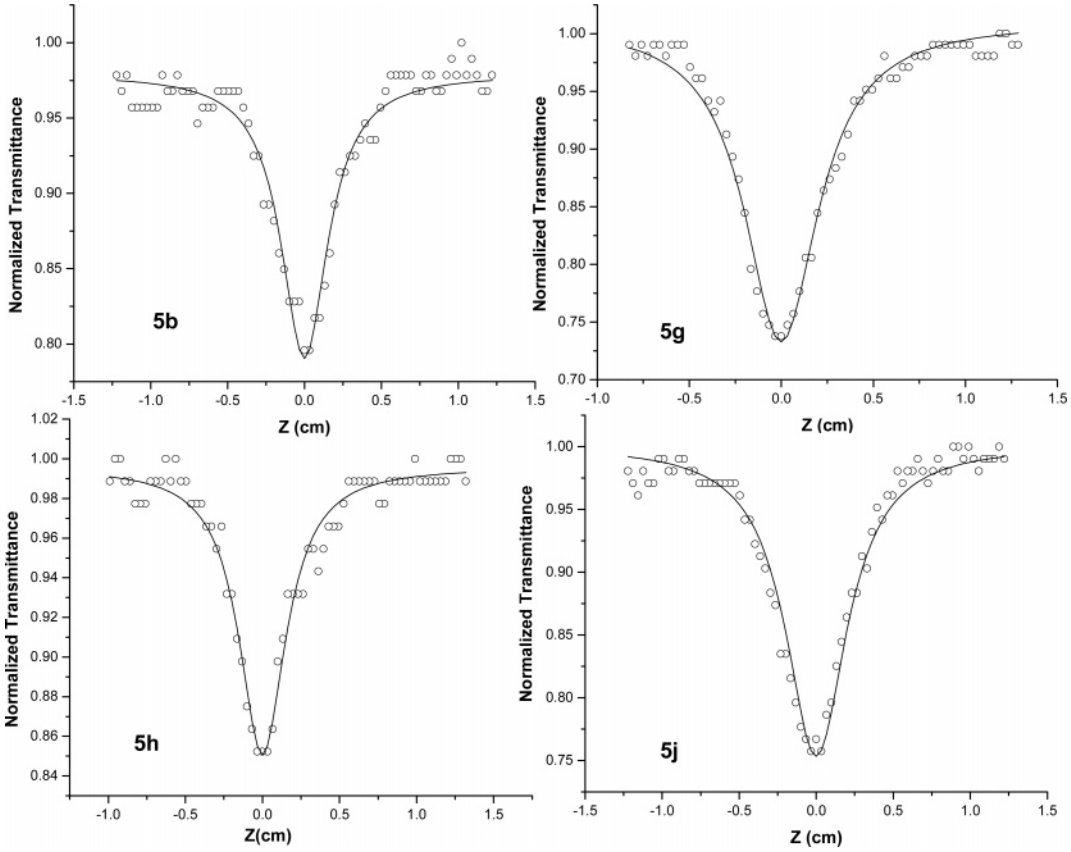

Figure 5. Open aperture *Z*-scan traces of **5b**, **5g**, **5h**, and **5j** in dichloromethane measured at a 150 fs pulse under the same experimental conditions. The sample concentration is 0.10 mM. The solid lines are the best-fitted curves of the experimental data.

ability of the ferrocene moiety. The smaller value of the θ twist in **4g** also enhances this electron donation from the substituent. Both the redox potential and TPA cross section data for **4g** support this observation. It may be noted from the V_{min} values that in all the rhodium-free systems the electron distribution is not homogeneous because the most electron-rich region (~32 kcal/mol) found on the **A** ring is nearly 3.6 times more negative than the most electron-deficient region on the furan moiety (~9 kcal/mol). However, this scenario is completely different in the rhodium-coordinated **5b** system because the V_{min} points in this system are found to be in the range of −12.1 to −18.5 kcal/mol (Figure 9b), suggesting a more uniform distribution of electrons in Rh(I)-coordinated systems than that of the free bases.

III. Discussion

With the above understanding of molecular and electronic structure it has been possible for us to understand the TPA cross section values and redox potential observed for conjugates and their Rh(I) derivatives. For convenience, the TPA cross section values for smaragdyrin with phenylacetylene spacers and smaragdyrin with ferrocenyl spacers are discussed separately. For the smaragdyrin with phenylacetylene groups the TPA cross section value increases linearly from **4a**−**4f**. This can be attributed to the increased conjugation upon going from **4a**−**4f**. Structurally the only difference upon going from **4a**−**4f** is the increase in the number of phenylacetylene spacers from two to three, which are linked through acetylenic bridges. Such a structural disposition is known to enhance the π conjugation.[15] Our theoretical study also supports this observation. Furthermore, recent results from the laboratory of Kim and Osuka have shown that effective π delocalization between the molecular partners in a large conjugated system enhances the TPA cross section values.[10a] Further, the para isomers show larger $\sigma^{(2)}$ values compared to those of the corresponding meta isomers. This is attributed to the disruption in the extended π conjugation for the meta isomer relative to that of the para isomer. The extension in conjugation depends upon the electronic interaction between smaragdyrin π system and the meso substituents. This in turn depends upon the dihedral angle of the meso substituents relative to the smaragdyrin plane. Theoretical study shows that the θ twist (Table 4) observed for para isomers is lower as compared to that of meta isomers, clearly suggesting the enhanced electronic interaction and hence larger TPA cross section values for para isomers. This is also supported by the observation of Kim and Osuka where larger $\sigma^{(2)}$ values were reported for the porphyrin dimers and trimers with the lower dihedral angle.[10a] The difference in the TPA cross section values at 780 and 830 nm is attributed to resonance enhancement at 830 nm.

For the ferrocene-linked smaragdyrins, the $\sigma^{(2)}$ values are higher relative to those of the phenylacetylene smaragdyrins. For the ferrocene systems the MESP surfaces are spread over the macrocycle, and the negative V_{min} are different over the benzene ring, the acetylenic bond, the smaragdyrin π system, and the cyclopentadienyl ring. From the MESP data one would expect a larger $\sigma^{(2)}$ value for **4g** in which ferrocene is linked directly to the π system relative to that of **4h** and **4i**, where ferrocene is linked with the phenyl spacers. The TPA cross section values of 5677 GM for **4g**, 3424 GM for **4h**, and 1803

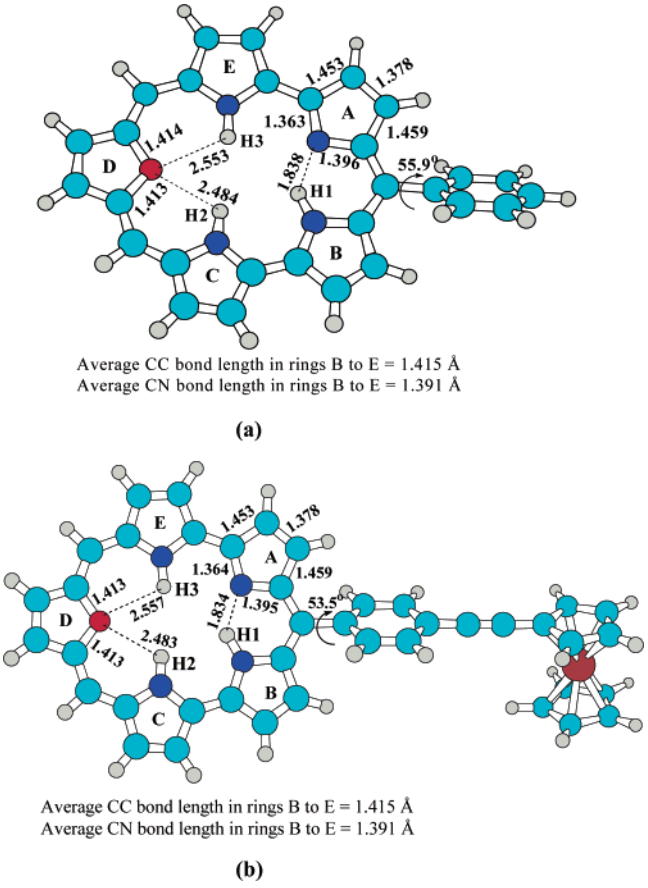

Figure 6. Optimized structure of (a) **4b** and (b) **4h** (for the Fe atom LanL2DZ and for the other atoms 6-31G(d) basis sets are used in the calculations). Some important bond lengths are shown in units of angstrom.

Table 4. Geometrical Features of Smaragdyrin Systems[a]

systems	N–H1	O–H2	O–H3	CC	CN	θ twist (deg)
4a	1.887	2.495	2.569	1.378	1.363	
4b	1.838	2.484	2.553	1.378	1.362	55.9
4c	1.836	2.483	2.552	1.378	1.364	53.3
4d	1.839	2.488	2.554	1.378	1.363	56.3
4e	1.835	2.483	2.551	1.378	1.364	52.9
4g	1.808	2.479	2.551	1.378	1.364	38.3
4h	1.834	2.483	2.557	1.378	1.364	53.5
4i	1.834	2.484	2.554	1.378	1.363	55.3

[a] CC_{ave} and CN_{ave} values were all within the small limit of 1.414−1.416 and 1.389−1.392 Å, respectively. The shortest CC and CN bonds observed on ring A are also given. All bond lengths are in angstrom.

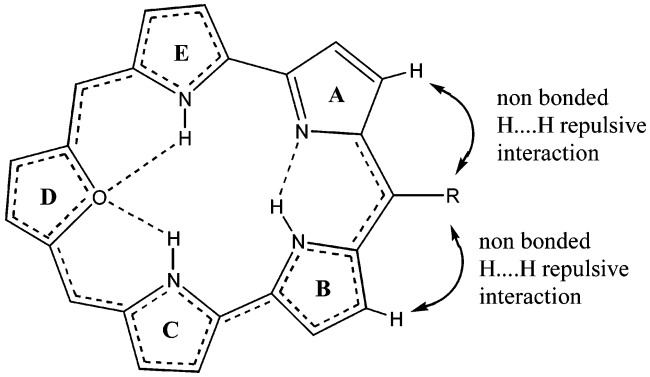

Figure 7. Schematic structure showing the electron delocalization/localization in the smaragdyrin system.

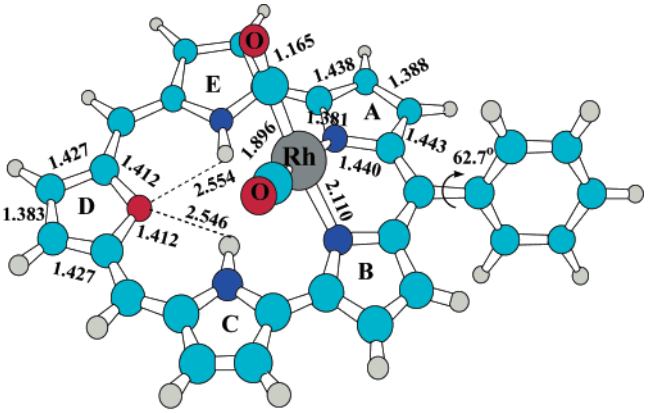

Figure 8. BLYP level optimized geometry of **5b** (for the Rh atom LanL2DZ and for the other atoms 6-31G(d) basis sets are used in the calculations). All bond lengths are in angstrom.

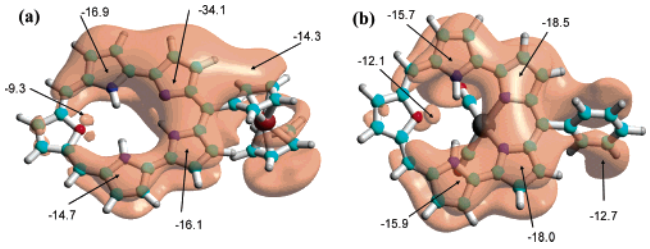

Figure 9. MESP isosurfaces of value −7.0 kcal/mol showing the extended π-electron conjugation in (a) **4g** and (b) **5b**. The values of the most negative-valued MESP (V_{min}) point (in kcal/mol) observed over various regions are also shown.

for **4i** are consistent with this observation. The lowering of the TPA cross section value of **4i** relative to that of **4h** is attributed to the location of the ferrocene link (for **4h** ferrocene link at para, for **4i** ferrocene at the meta position of phenyl). For ferrocene-linked systems **4j** and **4k** the $\sigma^{(2)}$ values are much more enhanced compared to those of **4g**. This can be attributed to the enhanced π conjugation because of the linking of the phenylacetylenylphenyl linker, relative to the simple phenyl linker. The effect of the para and meta linkage is also seen in the observed TPA cross section values (larger values for para isomers).

The Rh(I) derivatives in all cases show enhanced $\sigma^{(2)}$ values compared to those of the free-base derivatives. Both the HOMA index and MESP distribution described in the theoretical part suggest that in the Rh complexes the electron distribution is more homogeneous, unlike in the free bases, where electron delocalization is confined to only four of the five available heterocyclic rings. It may be noted that all the rhodium-coordinated systems selected in this study may show the planar tetra-coordinate geometry around the rhodium atom and a nearly planar smaragdyrin unit, very similar to that of **5b**.[17] Therefore, a high value of aromaticity is expected in all the "**5**" systems. This increased aromaticity is responsible for the large enhancement of the $\sigma^{(2)}$ values upon Rh(I) metalation. Our electrochemical data suggest harder ring oxidation of the smaragdyrin ring in the Rh derivatives. In fact, a good linear correlation (correlation coefficient 0.982) exists between the $E_{1/2}^{Ox}(2)$ values of the free base and the Rh(I) derivative of smaragdyrins (Figure 10). This observation suggests that the π electrons of the smaragdyrin unit are bound more tightly in the Rh(I) derivatives

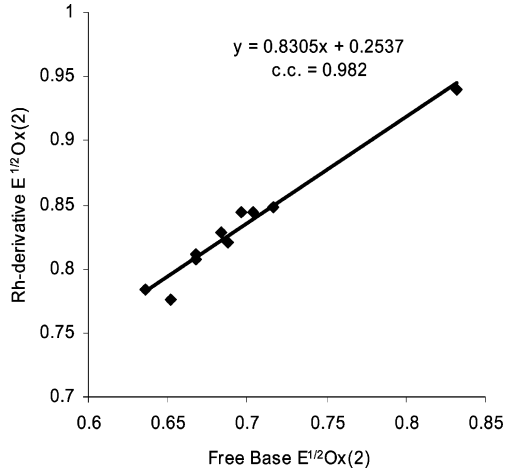

Figure 10. Correlation between the $E_{1/2}^{Ox}(2)$ values of free-base smaragdyrins and their Rh(I) derivatives.

relative to the free-base derivatives. The increased aromatic character of the Rh derivatives is consistent with this observation.

IV. Conclusion

We have described the synthesis and characterization of a series of 22π smaragdyrins with diverse meso substituents ranging from simple hydrogen to phenylacetylene and ferrocene. A simple [3 + 2] oxidative coupling methodology with the appropriate precursor has been applied for the synthesis. It has been shown that the optical, emission, and the electrochemical properties depend on the nature of the substituents, the linking group, and the spacer length. The TPA cross section $\sigma^{(2)}$ values measured for the free base as well as Rh(I) derivatives depend on the effective electronic communication between the smaragdyrin π system and the meso substituents. Large enhancements of the TPA values are observed upon introduction of Rh(I) metal to the smaragdyrin π system, due to the enhanced aromaticity. The theoretically calculated HOMA index data as well as the MESP distribution support the increased aromatic character in the Rh(I) smaragdyrins. Studies on the Rh(I) complexes of the other expanded porphyrins are in progress.

V. Experimental Section

All the synthetic procedures and experimental details are described in the Supporting Information.

Acknowledgment. T.K.C. thanks DST, New Delhi and D.G. thanks DST, MCIT, New Delhi and the International SRF program of Wellcome Trust, U.K. for financial support. R.M. and R.K. thank CSIR, New Delhi and A.N. thanks UGC, New Delhi for their fellowships.

Supporting Information Available: Synthetic procedures, measurement of the two-photon absorption cross section, computational method, optimized geometry, and MESP analysis of the **4a**−**4e**, **4g**, **4h**, **4i**, and **5b** systems. This material is available free of charge via the Internet at http://pubs.acs.org.

JA0628295